RESEARCH ARTICLE | DECEMBER 04 2020

Covalent incorporation of diphenylanthracene in oxotriphenylhexanoate organogels as a quasi-solid photon upconversion matrix

Special Collection: Up- and Down-Conversion in Molecules and Materials

Deise F. Barbosa de Mattos; Ambra Dreos; Mark D. Johnstone; August Runemark; Claire Sauvée; Victor Gray ; Kasper Moth-Poulsen ; Henrik Sundén ; Maria Abrahamsson

J. Chem. Phys. 153, 214705 (2020)
https://doi.org/10.1063/5.0029307

The Journal of Chemical Physics ARTICLE scitation.org/journal/jcp

Covalent incorporation of diphenylanthracene in oxotriphenylhexanoate organogels as a quasi-solid photon upconversion matrix

Cite as: J. Chem. Phys. 153, 214705 (2020); doi: 10.1063/5.0029307
Submitted: 11 September 2020 • Accepted: 11 November 2020 •
Published Online: 4 December 2020

Deise F. Barbosa de Mattos, Ambra Dreos, Mark D. Johnstone,[a] August Runemark, Claire Sauvée, Victor Gray,[b] Kasper Moth-Poulsen, Henrik Sundén,[c] and Maria Abrahamsson[d]

AFFILIATIONS

Department of Chemistry and Chemical Engineering, Chalmers University of Technology, Gothenburg, Sweden

Note: This paper is part of the JCP Special Topic on Up- and Down-Conversion in Molecules and Materials.
[a] **Present address:** Department of Chemistry, School of Science, Auckland University of Technology, Auckland, New Zealand.
[b] **Present address:** Department of Chemistry, Ångström Laboratory, Uppsala University, Box 523, 751 20 Uppsala, Sweden.
[c] **Present address:** Department of Chemistry and Molecular Biology, University of Gothenburg, 412 96 Gothenburg, Sweden.
[d] **Author to whom correspondence should be addressed:** abmaria@chalmers.se

ABSTRACT

Triplet–triplet annihilation photon upconversion (TTA-UC) in solid state assemblies are desirable since they can be easily incorporated into devices such as solar cells, thus utilizing more of the solar spectrum. Realizing this is, however, a significant challenge that must circumvent the need for molecular diffusion, poor exciton migration, and detrimental back energy transfer among other hurdles. Here, we show that the above-mentioned issues can be overcome using the versatile and easily synthesized oxotriphenylhexanoate (OTHO) gelator that allows covalent incorporation of chromophores (or other functional units) at well-defined positions. To study the self-assembly properties as well as its use as a TTA-UC platform, we combine the benchmark couple platinum octaethylporphyrin as a sensitizer and 9,10-diphenylanthracene (DPA) as an annihilator, where DPA is covalently linked to the OTHO gelator at different positions. We show that TTA-UC can be achieved in the chromophore-decorated gels and that the position of attachment affects the photophysical properties as well as triplet energy transfer and triplet–triplet annihilation. This study not only provides proof-of-principle for the covalent approach but also highlights the need for a detailed mechanistic insight into the photophysical processes underpinning solid state TTA-UC.

INTRODUCTION

In 1960, Shockley and Queisser[1] published the theoretical efficiency limit for single junction solar cells as ≈32%, a limit that comes about mainly due to the mismatch between the solar spectrum and the bandgap of the solar cell materials. A few years later, Parker and Hatchard published their seminal papers[2] on a phenomenon that today is considered a promising way to overcome the Shockley–Queisser limit, photon upconversion through triplet–triplet annihilation (TTA-UC).[3] In the TTA-UC process, two low energy photons are combined to form one high energy photon, enabling utilization of photons with lower energy than the solar cell bandgap.[4,5] Sensitized TTA-UC, schematically illustrated in Fig. 1, relies on a series of energy transfer reactions.[3,5–7] In short, a triplet excited sensitizer ($^3S^*$) is formed through photon absorption and intersystem crossing (ISC). The $^3S^*$ then interacts with a ground state annihilator (A_0) through a Dexter[8,9] type triplet–triplet energy transfer (TET) reaction yielding a triplet excited annihilator ($^3A^*$). Thereafter, two $^3A^*$'s interact in the triplet–triplet annihilation (TTA) process to form one singlet excited annihilator ($^1A^*$), which can release its excess energy as photons, and one ground state annihilator (A_0).

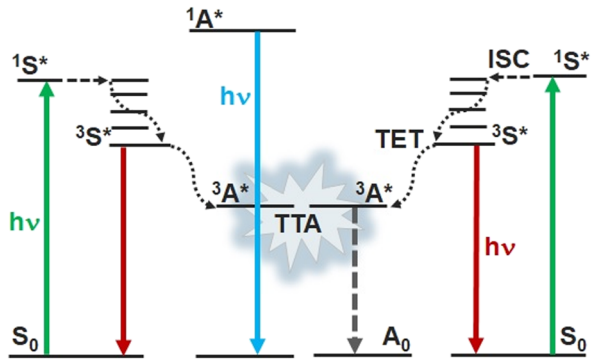

FIG. 1. Schematic illustration of the sensitized TTA-UC process. Green arrows represent photon absorption, and blue and red arrows represent photon emission as fluorescence and phosphorescence, respectively.

The specific requirements on sensitizers and annihilators have been extensively described elsewhere;[7] suffice it to say that the overall efficiency depends on the product of the quantum yields for each individual step. In liquid solution, efficient TET and TTA rely on diffusion[7,10] and are thus typically not a bottleneck in achieving efficient TTA-UC. In fact, overall quantum yields as high as 38%[11] (using a notation with the maximum quantum yield being 50%[12,13]) have been achieved. Moving into the solid state, which is required for successful incorporation into devices, has been slower due to a number of scientific challenges. These include ways to circumvent the molecular diffusion requirement and to overcome oxygen sensitivity.[7,14–18]

Attempts to achieve solid state TTA-UC have included crystalline solids,[19,20] polymers[21,22] and polymer films,[23–26] assemblies relying on coordination bonds,[27] bilayer solid state evaporated films,[28,29] and metal organic frameworks.[30–32] However, these approaches typically suffer from challenges with solubility,[22,23] aggregation,[20,26] poor exciton migration,[33] back energy transfer,[8,22,34] or self-quenching of the sensitizer.[23,26,35] An alternative strategy that has been proposed is to use a gel matrix since that allows for diffusion in the solvent pockets while still maintaining a macroscopic solid state.[7,36–40] In fact, TTA-UC has been observed in both organogels[36–38] and hydrogels,[41,42] sometimes with overall efficiencies close to those reported in liquid systems.[7,36–38] Typically, sensitizers and annihilators are mixed into the gel matrix, and detailed studies reveal only somewhat lower diffusion rates than those typically observed in the liquid state.[36] However, as noted by Kimizuka and others, this approach does not allow any control over the distance or orientation of chromophores. An appealing way to overcome this would be covalent incorporation of chromophores onto the gelators. As noted by Kimizuka and co-workers, such reports are scarce due to the elaborate and time-consuming multi-step synthesis schemes typically required.[38,43]

Here, we show that the above-mentioned issues can be overcome using the versatile and easily synthesized oxotriphenylhexanoate (OTHO) gelator[44–48] (Fig. 2). What makes the OTHO-gelator unique is that it allows covalent incorporation of chromophores (or other functional units) at well-defined positions. To study the self-assembly properties as well as its use as a TTA-UC platform, we combine the benchmark TTA-UC couple platinum octaethylporphyrin (PtOEP) as a sensitizer and 9,10-diphenylanthracene (DPA) as an annihilator, where DPA is covalently linked to the OTHO-gelator (Fig. 2). We show that TTA-UC can be achieved in the chromophore-decorated gel and that the position of attachment affects the photophysical properties as well as triplet energy transfer and triplet–triplet annihilation. This study not only provides proof-of-principle for the covalent approach but also highlights the need for a detailed mechanistic insight into the photophysical process underpinning solid state TTA-UC.

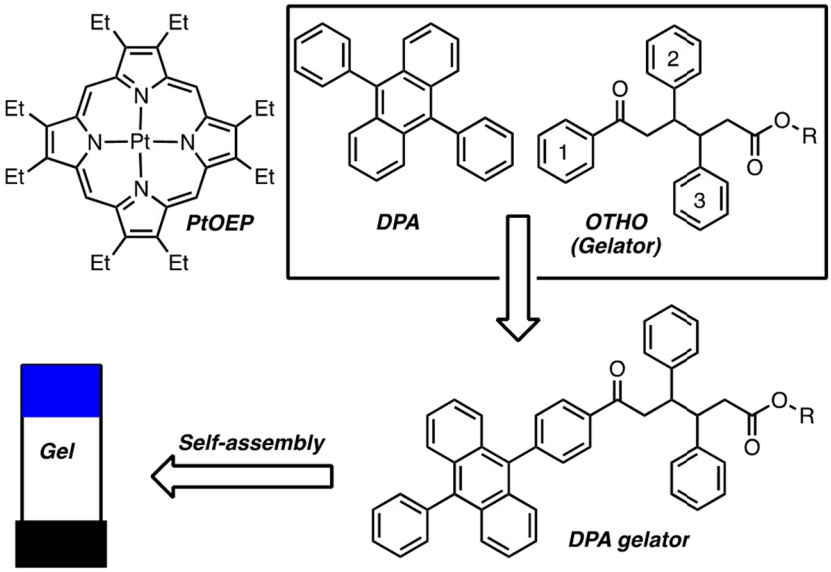

FIG. 2. Structural formulas of the sensitizer PtOEP, the annihilator DPA, and the OTHO-gelator, and the overall design scheme of DPA-decorated supramolecular gels.

RESULTS AND DISCUSSION

Gel synthesis and formation

The OTHO-molecule (Fig. 2) is a versatile gelator, developed by Ta *et al.*[44] It is easily synthesized in a multi-component reaction, and chromophores such as polyaromatic compounds can be installed on the aromatic rings with coupling reactions (see scheme S1 of the supplementary material for details). The self-assembly relies to a large extent on the aromatic rings 1 and 2 and thus assures the close proximity between chromophores required for TTA (Fig. 2).[45]

In this work, we chose to incorporate the annihilator into the gel structure, exploring the effect of different attachment points, as shown in Figs. 2 and 3. In total, three different structures were prepared, p1(PA)OTHO and p2(PA)OTHO, with DPA attached to aromatic ring No. 1 and No. 2, respectively, and p1p2$(PA)_2$OTHO that contains two DPA-moieties, one at each aromatic ring (Fig. 3). In addition, we investigated the unsubstituted OTHO (for the structure, see Scheme S1) with PtOEP and DPA mixed into the solution prior to gelation. For simplicity, we will henceforth refer to p1(PA)OTHO, p2(PA)OTHO, and p1p2$(PA)_2$OTHO as p1, p2, and p1p2, respectively.

All four OTHO derivatives readily formed gels in toluene, following dissolution in the hot solvent and cooling to room temperature, as expected based on previous results.[44,45] When DPA is dissolved in OTHO, turbid gels are formed (Fig. S1), which is also the case for p1 and p2 gels, suggesting that the formed gel fibers may be as large as on the order of 1 μm, in agreement with the previous studies.[45] p1p2 forms less turbid gels, indicating narrow gel fibers. This is not surprising as even subtle structural modifications can dramatically affect self-assembly and the resultant gel properties.[45,47] Addition of the sensitizer to the mixtures prior to gelation causes no visible difference to the turbidity of any of the samples.

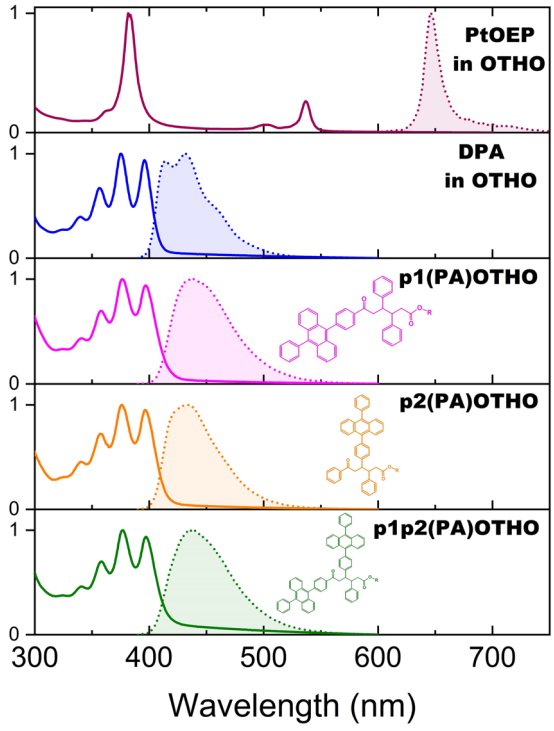

FIG. 3. Structures of p1, p2, and p1p2 together with normalized absorption (solid lines) and emission (dotted lines) spectra of the compounds used in this study in the gel matrix. Light scattering is evident in the red end and tails of the absorption spectra.

Photophysical characterization of OTHO samples

The absorption and emission spectra of PtOEP and DPA in OTHO are unremarkable and appear very similar to their respective solution spectra, as shown in Fig. 3.[49,50] The absorption spectra of the OTHO-DPA derivatives, as shown in Fig. 3, are also very similar to DPA in OTHO. The strong light scattering caused by the turbidity is evident in the tails to the red end of the spectra.

The emission spectra for the OTHO-DPA derivatives show the maximum intensity at the same wavelength as DPA in OTHO but are slightly broadened and no vibrational structure can be distinguished. These results confirm that covalent attachment of the DPA-moieties does not change the ground state electronic properties to any appreciable extent, in line with observations where OTHO has been decorated with other functionalities.[45] Due to turbidity, fluorescence quantum yields (Φ_{FA}) could not be reliably determined in the gels, and instead, they were measured in toluene solution (Table I and Fig. S2) using DPA in toluene as the standard, Φ_{FA} = 100%.[51] Interestingly, for p1 and p1p2, Φ_{FA} ~ 50%, while p2 exhibits a quantum yield close to 100%.

Furthermore, the gel samples were characterized using time-resolved emission. Time-correlated single photon counting measurements of DPA (Fig. S3) (λ_{exc} = 377 nm) in the OTHO gel revealed single exponential decay of the fluorescence (τ_{FA}), with a rate constant similar to what has been observed in solution,[51] as shown in Table I. The OTHO-DPA derivatives display the same trend for the radiative decay, as was observed for the quantum yield, and p2 exhibits mono-exponential decay and a fluorescence lifetime very similar to what was observed for DPA in OTHO. In contrast, p1 and p1p2 gels display double exponential decays, with average fluorescence lifetimes of around half of that of DPA in OTHO, in agreement with the observed fluorescence quantum yields. The reason for the increased non-radiative decay is not clear, but it appears that having the phenyl anthracene installed on aromatic ring 1 promotes non-radiative decay more than having it installed on aromatic ring 2.

PtOEP (6 μM) phosphorescence in the OTHO gel was monitored at 646 nm and revealed double exponential decay on the order of tens of μs, as shown in Table I. This is in contrast to the solution data where PtOEP displays a mono-exponential triplet lifetime (τ_{PS}) of 50 μs in deaerated toluene.[49] To better understand the biexponential decay, we compared high and low concentration samples (115 μM and 6 μM) and varied the excitation power, as shown in Table I. The decay is double exponential in all cases, and high excitation power appears to shorten the observed lifetime even more (Fig. S4). We attribute this behavior to triplet–triplet annihilation between the sensitizer molecules since high local concentrations in the gel can be easily imagined, and concentration-induced self-quenching has been previously reported for solution samples with

TABLE I. DPA fluorescence quantum yields (in toluene solution), DPA fluorescence lifetimes and amplitudes (A_1) in the OTHO gel (λ_{ex} = 377 nm and λ_{emis} = 432 nm); PtOEP phosphorescence lifetimes in the OTHO gel (λ_{ex} = 532 nm and λ_{emis} = 646 nm) at varying concentration and excitation power. Errors correspond to one standard deviation.

Compound	Φ_{FA}	$\tau_{FA,1}$ (ns) (A_1%)	$\tau_{FA,2}$ (ns)
DPA in OTHO	1.0[a]	6.5 ± 0.7	...
p1	0.52 ± 0.1[b]	2.7 ± 0.9 (60 ± 21)	3.6 ± 1.7
p2	0.92 ± 0.1[b]	7.1 ± 0.7	...
p1p2	0.51 ± 0.1[b]	2.6 ± 0.8 (60 ± 15)	3.4 ± 1.4

	(PtOEP) (μM)	Excitation power (mW)	$\tau_{PS,1}$ (μs) (A_1%)	$\tau_{PS,2}$ (μs)
PtOEP in OTHO	6	0.5	7.7 ± 4 (90 ± 4)	59.3 ± 8
		7	5.1 ± 3 (90 ± 4)	20.5 ± 12
	115	0.5	7.0 ± 4 (60 ± 11)	25.0 ± 22
		7	3.7 ± 0.5 (60 ± 11)	17.3 ± 12

[a]Value from Ref. 51.

[b]Quantum yields determined in toluene solution.

high enough concentration.[49] This competing process may be disadvantageous for the required triplet energy transfer between PtOEP and DPA.

Phosphorescence quenching in OTHO gels

The potential for TET was evaluated through concentration-dependent sensitizer phosphorescence quenching experiments followed by a Stern–Volmer type analysis.[52] The quenching efficiency is addressed through the relationship between the decrease in sensitizer emission intensity or excited state lifetime and the annihilator concentration according to[52]

$$\frac{I_0}{I} = \frac{\tau_0}{\tau} = 1 + k_{TET}\tau_0[\mathrm{A}], \tag{1}$$

where I_0 and I are the emission intensity without and with the annihilator, respectively, τ_0 and τ are the sensitizer phosphorescence lifetime without and with the annihilator present, and k_{TET} is the bimolecular quenching rate constant for the TET reaction. For purely dynamic quenching, a straight line with the same slope for the steady state and time resolved data is expected.

The PtOEP concentration was kept constant at 115 μM, and the effective DPA concentration was varied by mixing neat OTHO with p1, p2, and p1p2 to yield concentrations between 0 mM and 10 mM. The steady state and time resolved emission quenching data are available in Fig. 4 (see the supplementary material for details on how I_0/I, average lifetime, and τ_0/τ were determined). A qualitative analysis shows that free DPA in the OTHO gel quenches the PtOEP phosphorescence significantly more efficiently than any of the OTHO-DPA-derivatives. Furthermore, p1p2 is a more efficient quencher than p1 and p2.

A quantitative analysis of the quenching efficiencies was performed using the time-resolved data since they can be satisfactorily modeled with a linear relationship [Eq. (1)]. This analysis yields bimolecular rate constants for TET on the order of 0.5–2 × 10^8 M^{-1} s^{-1} for all OTHO-DPA derivatives and k_{TET} ~ 2 × 10^9 M^{-1} s^{-1} for DPA in OTHO (Tables II and S1). The latter value seems unexpectedly high, given that k_{TET} for the same sensitizer–annihilator pair in toluene has been reported to be 2.15 × 10^9 M^{-1} s^{-1}.[51] The high concentration of annihilators in the small solvent pockets may explain this observation, especially when contrasted to the findings in a study where free DPA and a Pd porphyrin were mixed into a 1,3:2,4-bis(3,4-dimethylbenzylidene) sorbitol/tetralin gel, and a quenching rate of 2 × 10^8 M^{-1} s^{-1} was reported.[36]

If we instead consider the steady state data, we note that both free DPA in OTHO and p1p2 show an upward curvature and that the steady state data result in larger ratios, as shown in Fig. 4. In the case of free OTHO in DPA, the I_0/I ratio is much larger at high concentrations than the τ_0/τ ratio. For p1p2, the upward curvature is less pronounced and the difference between the two ratios is less than a factor of 2. This type of deviation from Stern–Volmer behavior has been observed when both static quenching and dynamic quenching occur at the same time and also when fluorophore and quencher are in very close proximity, resulting in an apparent overestimation of the quenching rate.[52] In contrast, for p1 and p2, the steady state data are much more similar to the time-resolved ditto, but there is a tendency to reach a plateau at higher quencher concentrations. This kind of behavior has, for example, been observed when the fluorophore exists in distinctly different environments with varying accessibility to the quencher molecules as a consequence.

To better understand the discrepancies between time-resolved and steady state data for free DPA in OTHO, we followed the approach of Lakowicz[52] and analyzed the data with the combined static and dynamic quenching model (Fig. S6) resulting in the contributions of ~ 4 × 10^2 M^{-1} and ~ 1 × 10^4 M^{-1} for static and dynamic quenching, respectively. This means that apparent static quenching would account for roughly 3% of the quenching. Thus, it appears more probable that the observed behavior is due to the short distances between sensitizers and annihilators. The dynamic quenching appears high but may be explained by a very close proximity, as a result of small solvent pockets. Even though the most likely

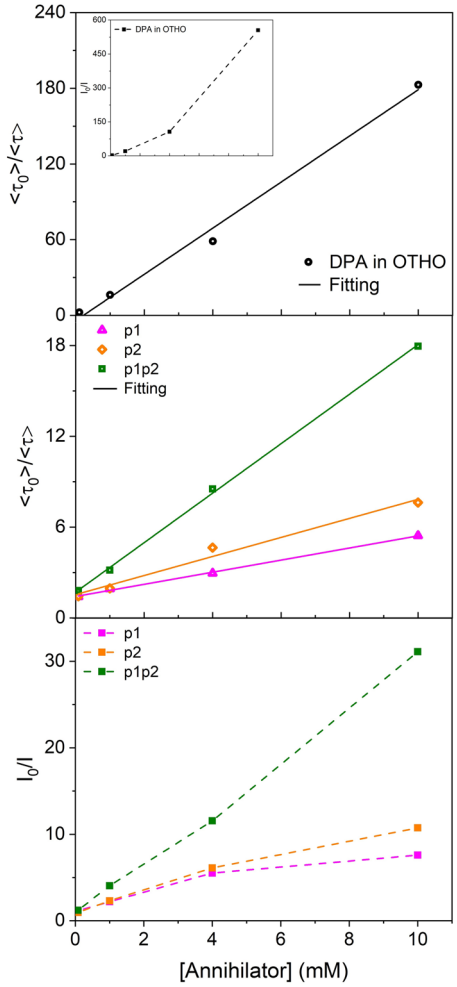

FIG. 4. Stern–Volmer plots of PtOEP phosphorescence quenching through TET by DPA-moieties. Solid lines are linear fits to the time-resolved $\langle\tau_0\rangle/\langle\tau\rangle$ data, and dashed lines are guides to the eye used for steady-state I_0/I data. The inset shows the steady-state data for DPA in OTHO, and the points refer to [DPA] = 0.1 mM, 1 mM, 4 mM, and 10 mM.

explanation for the observed behavior is close proximity in the solvent pockets, possible chromophore co-localization was addressed by examining samples with [DPA] = 10 mM, which were dried in a nitrogen filled glovebox and subjected to steady-state emission measurements. In all samples, the phosphorescence remained after drying (Fig. S7), suggesting no strong complex formation between the sensitizer and annihilator in the gel state. We also note that it is possible that the strong light scattering affects the steady state data and may contribute somewhat to the deviations from linearity.

Another interesting question when discussing the quenching is whether the difference in k_{TET} for the OTHO-DPA derivatives and free DPA in OTHO can be explained only by the fact that diffusion is hindered in the covalently bound samples. To address this,

TABLE II. TET rate constants extracted from the Stern–Volmer analysis (based on time-resolved data), theoretical quenching constants based on the Smoluchowski equation, and the estimated quenching efficiency f_q.

	k_{TET} ($\times 10^8$ M^{-1} s^{-1})	k_0 ($\times 10^{10}$ M^{-1} s^{-1})	f_Q (%)
DPA in OTHO	23	1.1	20
p1	0.5	0.56	0.88
p2	0.8	0.56	1.4
p1p2	2.0	0.56	3.6

we applied the Smoluchowski equation[52,53] to calculate the theoretical diffusion controlled rate constant, k_0, for the different cases, as shown in Table II (details in the supplementary material). By comparing the theoretical values with our obtained rate constants, we can conclude that for p1 and p2, the decrease in quenching efficiency f_Q, which is the fraction of collisions between the sensitizer and annihilator that are effective for TET, cannot be explained solely by rigidification of the matrix (Tables II and S1).

Given that p1p2 shows the highest quenching efficiency, one may speculate that the structure with DPA-units pointing in different directions and the narrower gel fibers of p1p2 make the DPA-units more accessible, resulting in a higher triplet energy transfer. The difference between p1 and p2 is too small to conclusively say that there is a real difference between the two. Taken together, the quenching studies highlight the complexity of the supramolecular assemblies and the need for further studies to understand this behavior in more detail.

Triple-triplet annihilation upconversion in OTHO samples

The overall TTA-UC process relies on both efficient TET and efficient triplet–triplet annihilation. The latter requires that two $^3A^*$ moieties are in close enough contact for the triplets to annihilate within the triplet lifetime. Here, our covalent approach presents a clear difference to TTA in solution since the annihilation process is no longer dependent on chromophores diffusing. Based on the previous results for TTA-UC in gel matrices, as well as the obtained TET rate constants and fluorescence quantum yields, it is reasonable to assume that free DPA in the OTHO will yield the highest overall efficiency, followed by p1p2, p2, and p1. Nanosecond transient spectroscopy, used to follow the build-up of the DPA fluorescence (Fig. S8 and Table S2), suggests, however, that free DPA in OTHO is ~2 orders of magnitude faster than the three OTHO-DPA derivatives, which behave similarly.

Figure 5 shows the steady state upconverted fluorescence, following excitation at 532 nm, with the DPA fluorescence centered around the 432 nm peak and the remaining PtOEP phosphorescence peak at 646 nm for samples containing 10 mM DPA units and 115 μM PtOEP. Comparing the relative intensities of the upconverted emission and the remaining sensitizer phosphorescence confirms that the overall TTA-UC process is much more efficient for free DPA than in the covalently bound OTHO-DPA derivatives.

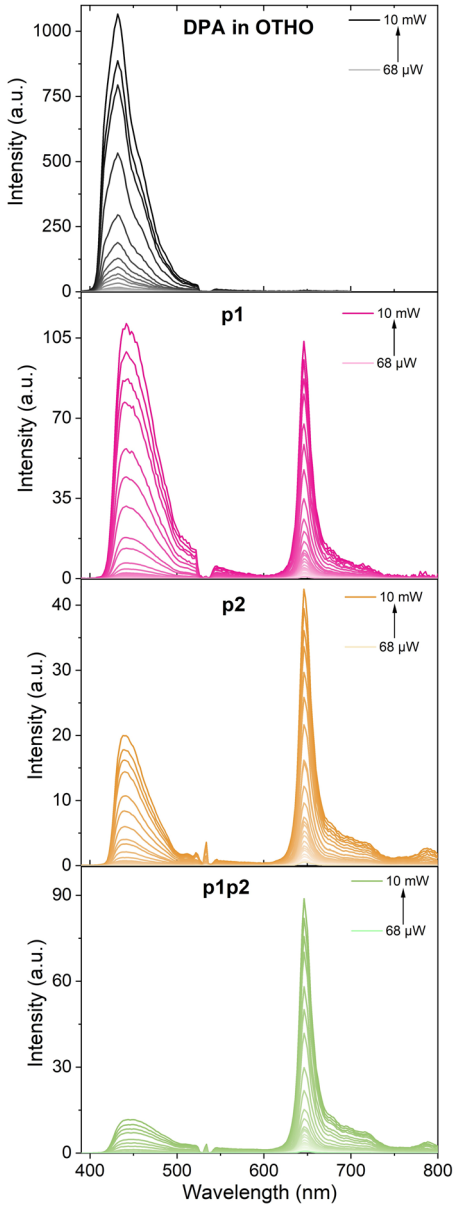

FIG. 5. Emission profiles of gel samples with varying excitation powers at 532 nm. The features between 400 nm and 525 nm correspond to upconverted fluorescence from DPA. Unquenched PtOEP phosphorescence is present at 646 nm. [PtOEP] = 115 μM, [DPA units] = 10 mM, and [OTHO units] = 10 mM.

Interestingly, p1p2 shows the lowest and p1 the highest upconversion intensity of the DPA-gelators, indicating that the triplet migration and TTA are more efficient in gels of p1 than p2 and p1p2. The same trend is observed in the upconverted fluorescence lifetime, as shown in Table S2.

To better understand the TTA-process in the gels, we also looked at a lower DPA-unit concentration, 4 mM (Fig. S9), by comparing with relative intensities at different concentrations. As judged by the relative intensity between the phosphorescence and upconverted fluorescence peaks, 10 mM is, as expected, more beneficial for free DPA in OTHO. The same is true for p1, while the 10 mM and 4 mM ratios are similar for p2. Finally, p1p2 shows a more efficient overall process at 4 mM.

The dried gel samples were also tested under the same conditions, and the upconverted emission is shown in Fig. S10. Upconverted fluorescence was observed for all samples, but the intensity drastically decreased. Interestingly, the largest difference between the gel and dry state is observed for free DPA and p1. Furthermore, we note an emission feature centered around ~775 nm (Fig. S7) that overlaps with what would be expected for excimer emission from PtOEP, presumably caused by aggregation.[49,56]

This is however only a qualitative analysis, and quantitative measures are required to build a more complete mechanistic picture. Upconversion efficiency is typically evaluated through the external quantum yield, usually measured in relation to another fluorophore with a known quantum yield.[7,11–13,54,55] However, the turbidity of the gels and the consequential light scattering, as well as the high concentrations used here, which cause significant inner filter effects, make reliable quantum yields hard to determine.[7]

Instead of evaluating the TTA-UC performance using the quantum yield, we looked at another important figure of merit, the intensity threshold I_{th}, i.e., the UC emission intensity dependence on the excitation power.[57] Typically, a log–log plot of UC intensity vs excitation power reveals two regimes, one in which UC emission to a first approximation is quadratically dependent on the excitation power and one regime where the concentration of $^3A^*$ is high enough that TTA effectively dominates and the relationship becomes linear.[6] The point where the lines cross is referred to as the intensity threshold (I_{th}) and is the minimum excitation power density needed to make TTA dominate the process.[6,57] This type of analysis is valid under the assumption of efficient TET, and this is easily achieved in solution, but it is not always the case in a solid matrix.[6] Here, however, the Stern–Volmer data suggest that TET is reasonably efficient and, indeed, 2 distinct regimes are visible for DPA in OTHO, p1, and p2, albeit not for p1p2, as shown in Fig. 6.

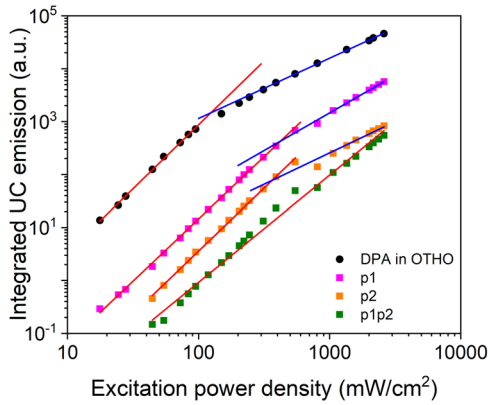

FIG. 6. Integrated upconversion efficiency as a function of excitation power for samples with [DPA-units] = 10 mM. The quadratic and linear regimes are indicated by the red and blue lines, respectively. The straight lines are results of a linear fit to the data.

The data shown in Fig. 6 could be satisfactorily modeled with two straight lines with slopes around 1 and 2 for all derivatives except p1p2 where only one regime (with a slope close to 2) was observed, as shown in Table III. For high excitation power densities, the slope shows small deviation from 1 when DPA is diffusing in OTHO; however, a high intensity threshold, 120 mW/cm^2, is observed. The same qualitative behavior is observed for p1 and p2; however, the upconverted emission intensity is much inferior, and the intensity thresholds are almost four times higher. No intensity threshold could be determined for p1p2 below an excitation power of 2500 mW/cm^2 (using higher excitation powers resulted in damage to the samples). The same analysis for 4 mM samples revealed similar I_{th}-values for free DPA in OTHO and p2, while 4 mM p1 showed a slightly lower threshold. For p1p2, no threshold value could be extracted at 4 mM.

Considering all the available data, it is expected that free DPA in OTHO should show the highest upconversion efficiency. This can be rationalized in terms of close proximity between sensitizers and annihilators in the solvent pockets. We cannot exclude that sensitizers or annihilators are to some extent localized in the gel fibers, but based on the solvent-like behavior, it is reasonable to assume that most of the TET and TTA occurs in the solvent pockets. In contrast, this opportunity is not available to the covalently bound DPA-OTHO derivatives, where exciton migration in the gel fibers is a prerequisite for efficient TTA. Given the striking difference between p1p2 and the other two, there must be a difference in behavior that cannot be explained by the photophysical properties. First, the structure is different with DPA units pointing in two different directions, which may result in a lower number of successful interactions between the two triplet excited annihilators. Second, as noted earlier, p1p2 appears to form narrower gel fibers than p1 and p2, possibly also leading to less efficient excitation migration. Understanding the difference between p1 and p2 is not as straightforward. The photophysical characterization revealed a higher fluorescence quantum yield for p2, and yet, p1 shows more efficient photon upconversion, despite similar TET rates, which leads to the conclusion that TTA must be more efficient in p1. The reason for this is not clear, but a speculation is that substitution on aromatic ring No. 1 leads to more efficient exciton migration. We cannot exclude that differences in gel properties may explain this, but that is beyond the scope of the current study.

Finally, the performance of our DPA-OTHO assemblies should be put in context by comparing with other gel-based approaches. First, however, a word of caution, it is well known that direct comparison of reported I_{th} or quantum yields may be misleading since experimental conditions have large impact on observed numbers. That said, PtOEP and DPA in toluene solution yield a reported I_{th} of 18 mW/cm^2,[51] which is a factor ~25 better than p1 and p2 and only a factor of 10 better than free DPA in OTHO. This relatively small difference between the solution and free DPA in OTHO strengthens our interpretation that both sensitizers and annihilators mostly reside in the solvent pockets of the gel. The threshold intensity reported here is close to the numbers observed by Vadrucci *et al.*[37] who studied DPA and a dicarboxylate derivative of palladium(II) mesoporphyrin IX in a organogel made of poly(vinyl alcohol) and hexamethylene diisocyanate in DMSO and found I_{th} of ca 100 mW/cm^2, which was assigned to the less efficient molecular diffusion. Another notable example is the same sensitizer–annihilator pair in a gel matrix formed by *N*,*N*′-bis(octadecyl)-L-Boc-glutamic diamide, where an I_{th} of 1.48 mW in air was reported and attributed to efficient annihilator exciton migration through the gel structure.[38] As noted in the Introduction, the type of covalently bound assemblies studied here is rare, which limits the number of relevant comparisons for p1, p2, and p1p2. One self-assembled system, which forms membrane like-structures in chloroform, reported an impressive I_{th} of 8.9 mW/cm^2.[55] These varying figures highlight the need for a better mechanistic understanding of both the TET and TTA processes in a gel matrix.

TABLE III. Value of the slopes from Fig. 6 and the intensity threshold.

Compound	Linear	Quadratic	I_{th} (mW/cm^2)
DPA in OTHO	1.1	2.4	120
p1	1.4	2.0	440
p2	1.2	2.4	390
p1p2	2.0		>1000

CONCLUSIONS

This work presents how we used OTHO, a low molecular weight gelator, to achieve quasi-solid state TTA-UC. The use of OTHO allowed control over the orientation and distance between chromophores, in this case, the annihilator, and also allowed investigation on how substitution at different positions affects the photophysical properties. For example, the attachment point affects the fluorescence quantum yield for DPA, which, in turn, impacts how well the molecule can perform the annihilation. Furthermore, it is clear that TET can be efficient enough to allow for useful TTA-UC, but that the structure of the gelator–chromophore molecule is important for performance. For example, one can hypothesize that narrower gel fibers in p1p2 facilitate TET since it creates a higher concentration of accessible DPA-motifs. For the TTA process to be efficient, two annihilators need to be in close enough contact within the lifetime of the triplet state. This requires either that the concentration of ^{3}DPA* is very high or that we have efficient exciton migration within the gel. Since TTA is more efficient in p1 and p2, it could imply that triplet migration in the fibers is quite inefficient, and also, we hypothesize that the structure of p1p2 results in an "apparent dilution" of the excited annihilator motifs, thus counteracting the more efficient TET. Efficient TTA appears to be one of the major bottlenecks for the systems studied here. A detailed study of the gel structure could reveal where the bottlenecks arise from and how better chromophore packing can be achieved. Taking all the results together, we can conclude that we have shown that we can successfully incorporate the annihilator covalently to the gelator in a simple synthesis and that TTA-UC can be achieved in organogels using a freely diffusing sensitizer.

SUPPLEMENTARY MATERIAL

See the supplementary material for details regarding synthesis and characterization, details about data treatment fitting procedures, and additional data.

ACKNOWLEDGMENTS

The Swedish Energy Agency is acknowledged for financial support of this work.

METHODS

Materials

Platinum Octaethylporphyrin (PtOEP) was purchased from PorphyChem; 9,10-Diphenylanthracene (DPA), toluene, and anhydrous toluene were purchased from Sigma Aldrich. The solvent was kept inside a nitrogen glovebox. All substances were used as received.

For synthesis of the OTHO derivatives, see the supplementary material.

Sample preparation

All samples were prepared in a 4 ml transparent glass vial. The vial was heated until complete dissolution of the gelator. The mixture was transferred, with a heated glass pipette, to a 1 mm quartz cuvette and the gel was promptly formed.[44,45]

For absorption, emission, and fluorescence lifetime of the annihilator, 0.4 ml of toluene was added to 1 mM DPA and 10 mM OTHO. For OTHO-DPA derivatives, the solvent was added to 1 mM of p1 or p2 and 9 mM OTHO. In order to have the same number of DPA units and gelator concentration, the solvent was added to 5 mM p1p2 and 5 mM OTHO.

For fluorescence quantum yield of p1, p2 and p1p2, a minimum amount of each compound was added to toluene, heated to dissolve and transferred to the cuvette. No gel formation or precipitation was observed.

The samples containing the sensitizer were prepared in a nitrogen glovebox with a stock solution of 115 μM PtOEP in anhydrous toluene. For absorption, emission, and phosphorescence lifetime of the sensitizer, 0.4 ml of the stock solution was added to 10 mM OTHO. For upconverting samples, the same volume of stock solution was added to a vial containing the gelator and annihilator. In all cases, the gelator concentration was always kept at 10 mM.

Spectroscopy

Absorption spectra were recorded using a Varian Cary 50 Bio UV–Vis spectrometer. Emission spectra were obtained in a Varian Cary Eclipse fluorescence spectrophotometer. For the annihilator fluorescence quantum yield, in p1, p2, and p1p2, a diluted solution of DPA in toluene was used as the reference (Φ_{fA} = 100%)[51] at 375 nm excitation.

The annihilator fluorescence lifetime was measured on a time correlated single photon counting (TCSPC) fluorescence spectrometer (Edinburgh Instruments) with a 377 nm PicoQuant picosecond laser diode and a 10 MHz repetition rate (collected at 432 nm in 4096 channels and stopped at 10 000 counts). The sensitizer phosphorescence lifetime was monitored at 646 nm with a home-built setup with a nanosecond pulsed Quanta-Ray Nd:YAG laser at 532 nm excitation. The setup is composed of the laser (10 Hz repetition rate and 10 ns FWHM), Spectra-Physics Primoscan OPO, Oriel Cornerstone monochromator, Applied Photophysics 5 stage PMT, and an oscilloscope.

Upconverted fluorescence emission measurements were performed using a home-built setup with a 532 nm Coherent Obis laser (0.07 mm diameter) and a SPEX 1681 spectrometer. To avoid the influence of the beam light, a notch filter was inserted between the sample and the spectrophotometer. For excitation power density dependence measurements, a neutral density filter was placed between the laser head and the sample. All reported results are the average of three independent measurements.

DATA AVAILABILITY

The data that support the findings of this study are available within the article and its supplementary material.

REFERENCES

[1] W. Shockley and H. J. Queisser, J. Appl. Phys. **32**, 510 (1961).
[2] C. A. Parker and C. G. Hatchard, Proc. Chem. Soc. **1962**, 386 (1962).
[3] D. V. Kozlov and F. N. Castellano, Chem. Commun. **2004**, 2860.
[4] P. Bharmoria, H. Bildirir, and K. Moth-Poulsen, Chem. Soc. Rev. **49**, 6529 (2020).
[5] J. De Wild, A. Meijerink, J. K. Rath, W. G. J. H. M. Van Sark, and R. E. I. Schropp, Energy Environ. Sci. **4**, 4835 (2011).
[6] D. Dzebo, K. Börjesson, V. Gray, K. Moth-Poulsen, and B. Albinsson, J. Chem. Phys. C **120**, 23397 (2016).
[7] V. Gray, K. Moth-Poulsen, B. Albinsson, and M. Abrahamsson, Coord. Chem. Rev. **362**, 54 (2018).
[8] Y. C. Simon and C. Weder, J. Mater. Chem. **22**, 20817 (2012).
[9] A. Monguzzi, R. Tubino, and F. Meinardi, Phys. Rev. B **77**, 155122 (2008).
[10] A. Nattestad, Y. Y. Cheng, R. W. Macqueen, T. F. Schulze, F. W. Thompson, A. J. Mozer, B. Fückel, T. Khoury, M. J. Crossley, K. Lips, G. G. Wallace, and T. W. Schmidt, J. Chem. Phys. Lett. **4**, 2073 (2013).
[11] S. Hoseinkhani, R. Tubino, F. Meinardi, and A. Monguzzi, Phys. Chem. Chem. Phys. **17**, 4020 (2015).
[12] Y. Zhou, F. N. Castellano, T. W. Schmidt, K. Hanson, ACS Energy Lett. **5**, 2322 (2020).
[13] V. Gray, D. Dzebo, M. Abrahamsson, B. Albinsson, and K. Moth-Poulsen, Phys. Chem. Chem. Phys. **16**, 10345 (2014).
[14] B. Joarder, N. Yanai, N. Kimizuka, and J. Chem, Phys. Lett. **9**, 4613 (2018).
[15] J.-H. Kim, F. Deng, F. N. Castellano, and J.-H. Kim, Chem. Mater. **24**, 2250 (2012).
[16] T. F. Schulze, J. Czolk, Y.-Y. Cheng, B. Fückel, R. W. Macqueen, T. Khoury, M. J. Crossley, B. Stannowski, K. Lips, U. Lemmer, A. Colsmann, and T. W. Schmidt, J. Chem. Phys. C **116**, 22794 (2012).
[17] K. M. Felter, M. C. Fravventura, E. Koster, R. D. Abellon, T. J. Savenije, and F. C. Grozema, ACS Energy Lett. **5**, 124 (2019).
[18] N. Nishimura, J. R. Allardice, J. Xiao, Q. Gu, V. Gray, and A. Rao, Chem. Sci. **10**, 4750 (2019).
[19] K. Kamada, Y. Sakagami, T. Mizokuro, Y. Fujiwara, K. Kobayashi, K. Narushima, S. Hirata, and M. Vacha, Mater. Horiz. **4**, 83 (2017).
[20] A. Monguzzi, R. Tubino, S. Hoseinkhani, M. Campione, and F. Meinardi, Phys. Chem. Chem. Phys. **14**, 4322 (2012).
[21] A. Monguzzi, M. Mauri, A. Bianchi, M. K. Dibbanti, R. Simonutti, and F. Meinardi, J. Chem. Phys. C **120**, 2609 (2016).

[22]X. Yu, X. Cao, X. Chen, N. Ayres, and P. Zhang, Chem. Commun. **51**, 588 (2015).
[23]S. H. Lee, J. R. Lott, Y. C. Simon, and C. Weder, J. Mater. Chem. C **1**, 5142 (2013).
[24]A. Monguzzi, R. Tubino, and F. Meinardi, J. Phys. Chem. A **113**, 1171 (2009).
[25]C. Li, C. Koenigsmann, F. Deng, A. Hagstrom, C. A. Schmuttenmaer, and J.-H. Kim, ACS Photonics **3**, 784 (2016).
[26]H. Goudarzi and P. E. Keivanidis, ACS Appl. Mater. Interfaces **9**, 845 (2017).
[27]V. Gray, B. Küçüköz, F. Edhborg, M. Abrahamsson, K. Moth-Poulsen, and B. Albinsson, Phys. Chem. Chem. Phys. **20**, 7549 (2018).
[28]M. Wu, D. N. Congreve, M. W. B. Wilson, J. Jean, N. Geva, M. Welborn, T. Van Voorhis, V. Bulović, M. G. Bawendi, and M. A. Baldo, Nat. Photonics **10**, 31 (2016).
[29]L. Nienhaus, J.-P. Correa-Baena, S. Wieghold, M. Einzinger, T.-A. Lin, K. E. Shulenberger, N. D. Klein, M. Wu, V. Bulović, T. Buonassisi, M. A. Baldo, and M. G. Bawendi, ACS Energy Lett. **4**, 888 (2019).
[30]S. Gharaati, C. Wang, C. Förster, F. Weigert, U. Resch-Genger, and K. Heinze, Chem. Eur. J. **26**, 1003 (2020).
[31]M. Hosoyamada, N. Yanai, K. Okumura, T. Uchihashi, and N. Kimizuka, Chem. Commun. **54**, 6828 (2018).
[32]J. M. Rowe, J. Zhu, E. M. Soderstrom, W. Xu, A. Yakovenko, and A. J. Morris, Chem. Commun. **54**, 7798 (2018).
[33]S. Raišys, K. Kazlauskas, S. Juršėnas, and Y. C. Simon, ACS Appl. Mater. Interfaces **8**, 15732 (2016).
[34]P. C. Boutin, K. P. Ghiggino, T. L. Kelly, and R. P. Steer, J. Chem. Phys. Lett. **4**, 4113 (2013).
[35]R. Vadrucci, C. Weder, and Y. C. Simon, J. Mater. Chem. C **2**, 2837 (2014).
[36]K. Sripathy, R. W. Macqueen, J. R. Peterson, Y. Y. Cheng, M. Dvořák, D. R. Mccamey, N. D. Treat, N. Stingelin, and T. W. Schmidt, J. Mater. Chem. C **3**, 616 (2015).
[37]R. Vadrucci, C. Weder, and Y. C. Simon, Mater. Horiz. **2**, 120 (2015).
[38]P. Duan, N. Yanai, H. Nagatomi, and N. Kimizuka, J. Am. Chem. Soc. **137**, 1887 (2015).
[39]P. Duan, D. Asthana, T. Nakashima, T. Kawai, N. Yanai, and N. Kimizuka, Faraday Discuss. **196**, 305 (2017).
[40]X. Liu, J. Fei, P. Zhu, and J. Li, Chem. Asian J. **11**, 2700 (2016).
[41]P. Bharmoria, S. Hisamitsu, H. Nagatomi, T. Ogawa, M.-A. Morikawa, N. Yanai, and N. Kimizuka, J. Am. Chem. Soc. **140**, 10848 (2018).
[42]C. Ye, J. Ma, S. Chen, J. Ge, W. Yang, Q. Zheng, X. Wang, Z. Liang, and Y. Zhou, J. Chem. Phys. C **121**, 20158 (2017).
[43]N. Yanai and N. Kimizuka, Chem. Commun. **52**, 5354 (2016).
[44]L. Ta, A. Axelsson, J. Bijl, M. Haukka, and H. Sundén, Chem. Eur. J. **20**, 13889 (2014).
[45]M. D. Johnstone, C.-W. Hsu, N. Hochbaum, J. Andréasson, and H. Sundén, Chem. Commun. **56**, 988 (2020).
[46]A. Axelsson, L. Ta, and H. Sundén, Catalysts **5**, 2052 (2015).
[47]C. Sauvée, A. Ström, M. Haukka, and H. Sundén, Chem. Eur. J. **24**, 8071 (2018).
[48]C.-W. Hsu, C. Sauvée, H. Sundén, and J. Andréasson, Chem. Sci. **9**, 8019 (2018).
[49]A. K. Bansal, W. Holzer, A. Penzkofer, and T. Tsuboi, Chem. Phys. **330**, 118 (2006).
[50]V. Gray, A. Dreos, P. Erhart, B. Albinsson, K. Moth-Poulsen, and M. Abrahamsson, Phys. Chem. Chem. Phys. **19**, 10931 (2017).
[51]V. Gray, D. Dzebo, A. Lundin, J. Alborzpour, M. Abrahamsson, B. Albinsson, and K. Moth-Poulsen, J. Mater. Chem. C **3**, 11111 (2015).
[52]J. R. Lakowicz, *Principles of Fluorescence Spectroscopy* (Springer science & business media, 2013).
[53]A. Fuliński, Acta Phys. Pol., B **29**, 1523 (1998).
[54]N. Yanai, K. Suzuki, T. Ogawa, Y. Sasaki, N. Harada, and N. Kimizuka, J. Phys. Chem. A **123**, 10197 (2019).
[55]T. Ogawa, N. Yanai, A. Monguzzi, and N. Kimizuka, Sci. Rep. **5**, 10882 (2015).
[56]F. Nifiatis, W. Su, J. E. Haley, J. E. Slagle, and T. M. Cooper, J. Phys. Chem. A **115**, 13764 (2011).
[57]A. Haefele, J. Blumhoff, R. S. Khnayzer, and F. N. Castellano, J. Chem. Phys. Lett. **3**, 299 (2012).